

Effect of Temperature on Synthesis of Hydroxyapatite/Chitosan Composite Using the *In-Situ* Method as a Heavy Metal Adsorbent

Novesar Jamarun*, Tri Yupi Amirullah, Syukri Syukri, Arika Prasejati, Wulandari Wulandari, Sintia Caniago, and Nabiila Ayyu Trycahyani

Department of Chemistry, Faculty of Mathematics and Natural Sciences, Universitas Andalas, Limau Manis, Padang 25163, Indonesia

* **Corresponding author:**

email: novesarjamarun@sci.unand.ac.id

Received: February 2, 2024

Accepted: May 23, 2024

DOI: 10.22146/ijc.93816

Abstract: Removing hazardous non-organic waste containing heavy metals like copper and lead is crucial for environmental protection. Adsorption offers a promising solution, with hydroxyapatite (HAp) serving as a biocompatible adsorbent due to its active surface area. However, its mechanical limitations necessitate enhancement through compositing with chitosan (CTS), a natural biopolymer. This study synthesized hydroxyapatite from cuttlefish bone as a calcium source, while chitosan was extracted from shrimp shells. The hydroxyapatite/chitosan (HAp/CTS) composites were prepared in situ at varying temperatures (55, 60, 65, 70, and 75 °C). The composites were characterized using FTIR, XRD, SEM, and SAA. The result indicated successful integration of HAp and CTS, with a crystallite size of 13.82 nm in the 65 °C composite. Based on SEM-EDS analysis, the HAp/CTS 65 °C morphology was agglomerated chunk particles with a Ca/P ratio of 1.61. The highest adsorption capacity value is found in the HAp/CTS 65 °C composite for both ions, 1.9979 mg/g for Cu²⁺ ions and 0.9965 for Pb²⁺ ions. The reusability test results of the HAp/CTS 65 °C composite succeeded up to two cycles. This research proves that the adsorption of Cu²⁺ and Pb²⁺ ions by HAp/CTS composite adsorbent has been successfully carried out.

Keywords: adsorption; chitosan; cuttlefish bone; hydroxyapatite; reusability

■ INTRODUCTION

Water pollution is one of the problems that is often encountered. Liquid or solid waste dumped into water without treatment is a severe problem for living organisms [1]. Some activities that are sources of water pollution are increasing, i.e., human population, industrial activities, agriculture, domestic waste, and mining. Waste from industrial activities can be the primary source of heavy metal pollution entering the water ecosystem. The consequences of these activities are hazardous because the waste accumulates and cannot be degraded in living organisms [2]. Currently, metals with toxic properties are often found because they are widely used in industry. Some heavy metals that are sources of water pollution are copper (Cu), lead (Pb), zinc (Zn), chromium (Cr), mercury (Hg), cadmium (Cd), and arsenic (As) [3].

On the other hand, living organisms require varying amounts of metals for metabolic processes. However, increasing the amount will disrupt metabolism and be toxic. Cu metal is an essential ingredient in making fertilizer, and the human body functions to produce hemoglobin. Meanwhile, Cu metal can be found in agricultural activities, jewelry, lunch boxes, recycled PVC lead paints, and lead batteries [3-4]. Therefore, heavy metal ions removal from wastewater has been widely researched over the past few years. Several physical and chemical processes exist, including precipitation, solvent extraction, membrane processes, filtration, ion exchange, and adsorption. Among them, adsorption is an efficient and economical process [5]. The efficiency of this technique depends on the nature of the adsorbent. Some adsorbents that have been employed are such as activated carbon, chitosan, and hydroxyapatite [6-8].

HAp material can be used as a natural adsorbent in treating wastewater contaminated with heavy metals. HAp is proven efficient in removing toxic metal ions such as Pb, Co, Ni, Cu, Zn, Cd, and uranium in aqueous solutions [9-10]. This material has advantages such as ion exchange capabilities originating from its structure, thermal stability, low solubility in water, high adsorption capacity for many pollutants, and environmental friendliness [11]. However, this material also has disadvantages, namely its instability under extreme conditions and difficulty removing the adsorbent after the adsorption process. Therefore, additional materials are needed to make a composite that can overcome this deficiency. Chitosan has non-toxic properties, good stability, and biocompatibility. Chitosan has hydroxyl (-OH) and amine (-NH₂) groups along the polymer chain, which is very effective at adsorbing dyes and metal ions [12].

In this research, a HAp/CTS composite has been made using the sol-gel method as an adsorbent for Cu²⁺ and Pb²⁺ metal ions. The sol-gel method has advantages over other methods because it is easy to do, produces high purity, and the temperature is relatively low [13]. The source of HAp comes from cuttlefish bones because this material contains 80–90% CaCO₃ and CTS comes from shrimp shells, which contain 20–30% chitin, which will later be processed into CTS [14]. The effect of temperature in the synthesis of HAp/CTS composites was investigated to determine the ability of significant adsorption to absorb pollutants. Research conducted on HAp-zeolite synthesis with the effect of temperature found that the higher the temperature, the crystallinity tends to increase, and the pore size distribution is in the mesoporous range, which is favorable for contaminant absorption [15]. Temperature variations were conducted at 50, 55, 60, 65, and 70 °C to determine the optimum temperature for composite synthesis. Afterward, the composites will be tested as adsorbents for Cu²⁺ and Pb²⁺ metal ions.

■ EXPERIMENTAL SECTION

Materials

The materials used in this research were cuttlefish bones (*Sepia* sp.), shrimp shells, nitric acid (HNO₃, 65%, Merck), diammonium hydrogen phosphate

((NH₄)₂HPO₄, Merck), ammonium hydroxide, (NH₄OH, 25%, Merck), sodium hydroxide (NaOH, Merck), hydrochloric acid (HCl, 37%, Merck), aquadest, acetic acid (CH₃COOH, 100%, Merck), copper(II) nitrate trihydrate ((Cu(NO₃)₂·3H₂O, Merck), lead(II) nitrate (Pb(NO₃)₂, Merck).

Instrumentation

The content of an element using X-ray fluorescence (XRF, PANalytical). Functional groups were determined using a Fourier transform infrared spectrometer (FTIR, Shimadzu) at wavenumbers 500–4000 cm⁻¹. The crystal structure was determined using an X-ray diffractometer (XRD, PANalytical). Surface morphology and elemental composition determination using scanning electron microscope-energy dispersive X-ray spectroscopy (SEM/EDX, Hitachi Flexsem). A surface area analyzer (SAA, TriStar II Plus Version 3.01) was used to determine the surface area. Concentration of Cu²⁺ and Pb²⁺ was measured using atomic absorption spectroscopy (AAS, 240FS AAS).

Procedure

CaO preparation from cuttlefish bones

CaO was prepared by washing the cuttlefish bones until clean and then air-drying them for 2–3 d. Next, the cuttlefish bones are ground with a grinder, and the bone powder is obtained. Cuttlefish bone powder was calcined at 900 °C for 5 h to get CaO powder [16].

Synthesis of HAp using the sol-gel method

About 4.2 g of CaO powder was dissolved in 75 mL of 2 M HNO₃ and then stirred using a magnetic stirrer at 65 °C for 15 min with a stirring speed of 250 rpm. Then, it was filtered, and the resulting Ca(NO₃)₂ solution was added to the NH₄OH solution until it reached pH 10. The Ca(OH)₂ solution was obtained. The Ca(OH)₂ sol was added with 0.18 M (NH₄)₂HPO₄ solution dropwise (250 mL) at 60 °C while stirring for 5 h until HAp solution was formed. The HAp solution is filtered and dried using an oven at 110 °C for 5 h, then calcined at 600 °C for 3 h [16].

Synthesis of CTS from shrimp shells

CTS synthesis begins by washing and drying the shrimp shells. Next, the shrimp shells are ground into

powder and sieved with a 60 mesh. The CTS synthesis process consists of three stages: deproteination, demineralization, and deacetylation [17]. An amount of 30 g of shrimp shell powder was weighed and mixed with 1 M NaOH solution with a powder-to-solvent ratio of 1:5 (w/v) for 20 h at room temperature (28 ± 2 °C). The mixture was filtered and washed with distilled water until the pH was neutral. The solid was dried at 60 °C for 30 min and weighed [18-19]. The deproteinized powder was mixed with 1 M HCl in a 1:5 (w/v) ratio for 16 h at 28 ± 2 °C. The mixture was filtered, and the product was washed with distilled water until the pH was neutral. Next, the chitin was dried at 60 °C for 30 min. The chitin yield obtained was then weighed. The chitin yield was mixed with NaOH (50% (w/v)) with a ratio of 1:10 (w/v) at 60 °C for 20 h to remove the acetyl groups, and CTS was produced. Next, the mixture was filtered and washed with distilled water until the pH was neutral. The CTS yield obtained was then dried for 4 h in an oven at 65 °C and weighed [18-19].

In-situ synthesis of HAp-CTS composite

The HAp/CTS composite was synthesized by weighing 1.40 g of CaO and dissolving it in 25.00 mL of 2.00 M HNO₃, then filtered and stirred for 15 min. In a separate beaker, 1.98 g of (NH₄)₂HPO₄ were dissolved and homogenized in 75.00 mL of distilled water. The (NH₄)₂HPO₄ solution was added to the CaO solution dropwise until the Ca/P molar ratio was 1.67. An amount of 0.60 g of CTS powder was dissolved in 50.00 mL of 2% acetic acid solution. Next, the CTS solution is added to the HAp solution and stirred. Adjust the pH of the mixture by adding NH₄OH p.a. solution until it reaches pH 11. The mixture is stirred at 60 °C for 3 h. Next, the mixture was filtered and dried using an oven at 60 °C for 24 h. The same was done for temperature variations in mixing the HAp/CTS composite, namely with temperature variations of 55, 60, 65, 70, and 75 °C [20].

Determination of adsorption capacity of HAp/CTS composites

The HAp/CTS composite used as an adsorbent in the absorption of Cu²⁺ and Pb²⁺ ion solutions must first be tested for adsorption capacity. The Cu²⁺ and Pb²⁺ ion solutions of 20 and 10 mg/L, respectively were pipetted in

10 mL and then put into an Erlenmeyer flask; the pH of the solution was adjusted to 6. An amount of 0.1 g of HAp/CTS 65 °C composite was put into the Cu²⁺ and Pb²⁺ solution. Next, stir at 200 rpm for 120 min. Then, the mixture was filtered through a 0.45 µm microporous membrane, and the absorbance of the filtrate was measured using an AAS at a wavelength of 324.7 and 283.3 nm for Cu²⁺ and Pb²⁺, respectively. It was also carried out in the same way on HAp/CTS 55, 60, 70, 75 °C, and HAp composites. Next, the adsorption capacity was calculated for each HAp/CTS composite with these temperature variations [21-24].

Determination of the adsorption isotherm of Cu²⁺ and Pb²⁺ solutions

Determination of the adsorption isotherm of the Cu²⁺ and Pb²⁺ solution was carried out by pipetting 10 mL of a 200 mg/L Cu²⁺ and Pb²⁺ ion solution, then adjusting the pH of the solution to 6. An amount of 0.1 g of HAp/CTS 65 °C composite was added to the Cu²⁺ and Pb²⁺ solution. Next, the mixture was stirred at 200 rpm for 120 min. After that, the mixture was filtered through a 0.45 µm microporous membrane, and the absorbance of the filtrate was measured using an AAS. The same treatment was carried out at concentrations of 400, 600, 800, and 1000 mg/L [23-24].

Determination of adsorption kinetics of Cu²⁺ and Pb²⁺ solutions

Determination of adsorption kinetics of Cu²⁺ and Pb²⁺ solutions was carried out by pipetting Cu²⁺ and Pb²⁺ solutions with concentrations of 20 and 10 mg/L as much as 10 mL, respectively, then put into an Erlenmeyer, and adjusted the pH of the solution to 6. The 65 °C HAp/CTS composite, as much as 0.1 g was put into the Cu²⁺ and Pb²⁺ solution. Then, the mixture was stirred at 200 rpm for 120 min. After that, the mixture was filtered through a 0.45 µm microporous membrane, and the absorbance of the filtrate was measured using an AAS. The same treatment was carried out at 30, 60, 90, and 150 min [23-24].

Reusability

Reusability was carried out by pipetting 10 mL of Cu²⁺ and Pb²⁺ solutions with concentrations of 20 and 10 mg/L, respectively, put into an Erlenmeyer, and

adjusted the pH of the solution to 6. An amount of 0.1 g of HAp/CTS 65 °C composite was added to the Cu²⁺ and Pb²⁺ ion solution. The mixture was stirred at 200 rpm for 120 min. Then, the mixture was filtered through 0.45 µm microporous membrane, and the filtrate was analyzed by AAS. The composite was washed with distilled water to remove the Cu²⁺ and Pb²⁺ solutions and then dried. The HAp/CTS composite was re-contacted with Cu²⁺ and Pb²⁺ solutions for several cycles [24-25].

■ RESULTS AND DISCUSSION

Analysis of the Chemical Composition in Cuttlefish Bones

The percentage of CaO content in cuttlefish bones was 96.561%. Its characterization using X-ray fluorescence is shown in Table 1. This compound has the potential to be used as a calcium precursor in the synthesis of HAp. Calcination of cuttlefish bones aims to remove substances in the form of carbonates and hydroxides into substances in the form of oxides. The coloration of the calcination residue was completely white. It shows no further degradation of organic compounds. Previous research showed that completely white residue with a crystalline phase in eggshell calcined at 900 °C [24]. The reactions in the calcination process is shown in Eq. (1) [25]:



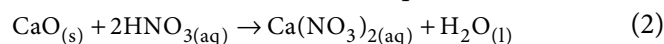
CTS Analysis

The result of the CTS obtained was 11.71 g, with the initial shrimp shell weighing 42.18 g. The CTS synthesis process starts with shrimp shells' deproteination and demineralization steps. This step is the process of obtaining chitin. Then, the deacetylation stage is the process of transforming chitin into CTS [26]. The deproteination process uses NaOH solution to remove the protein in the shrimp shell, characterized by foam and brown solution formation [19]. After the deproteination stage, the demineralization process is continued using a HCl solution to dissolve inorganic compounds in CaCO₃, characterized by air bubbles on the surface. The last stage, the deacetylation process using NaOH with a high concentration, aims to release the acetyl group on chitin

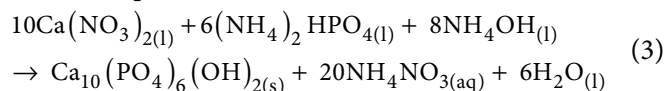
so that CTS with a high concentration is obtained [27]. The CTS obtained is a creamy white powder, as shown in Fig. 1(a).

Analysis of HAp-CTS Composite

The yield of HAp obtained using 4.2 g of CaO powder was 73.44% with a mass of 5.5299 g of HAp. The formation reaction is shown in Eq. (2) [28]:



The (NH₄)₂HPO₄ was added to the Ca(NO₃)₂ solution until Ca/P was 1.67. Then NH₄OH p.a was added with pH 11, the optimum pH of HAp sol formation. The white sol was dried and calcined to form pure HAp (Fig. 1(b)). The HAp-creating reaction is as follows (Eq. (3)) [28]:



The Effect of Temperature on HAp/CTS Composite

The HAp/CTS composites with temperature variations were obtained through an *in-situ* synthesis process. The mass of resulting products can be seen in Table 2. Based on Table 2, HAp/CTS 65 °C has a higher mass, which is correlated with the effectivity when applied to be adsorbent. At all temperature variations, the HAp/CTS composite is yellowish-white. It is due to

Table 1. The result of XRF characterization in cuttlefish bone

Component	Composition (%)
CaO	96.561
P ₂ O ₅	0.759
SO ₃	0.596
Al ₂ O ₃	0.294
Fe ₂ O ₃	0.132
Other	1.658



Fig 1. (a) Chitosan and (b) hydroxyapatite powder

Table 2. Effect of temperature to mass of HAp/CTS composites with temperature variations

Composite	Mass (g)
HAp/CTS 55 °C	2.950
HAp/CTS 60 °C	4.000
HAp/CTS 65 °C	4.190
HAp/CTS 70 °C	3.350
HAp/CTS 75 °C	3.190

the distribution of CTS in the HAp matrix. At higher temperatures, crystallization usually proceeds faster, which can affect the size and orientation of crystals in the composite.

The process of synthesizing HAp/CTS composites *in situ* is almost the same as synthesizing HAp. Still, in the synthesis of HAp/CTS composites *in situ*, the pH is adjusted after adding the CTS solution. This is so that the reaction process of HAp and CTS is formed simultaneously. The CTS was dissolved using a 2% acetic acid solution. The function of adding acetic acid is due to the presence of a carboxyl group ($-\text{COOH}$) in acetic acid, which then forms a hydrogen bond.

Determination of Adsorption Capacity of HAp/CTS Composite

The adsorption capacity of HAp/CTS composites is determined by the amount of adsorbate that can accumulate on the adsorbent surface. The maximum adsorption capacity can be obtained after optimizing the parameters that affect adsorption. Several factors affect adsorption: pH, temperature, adsorbent mass, solution concentration, contact time, adsorbent surface area, and adsorbent pore structure. The adsorbent was HAp/CTS composite with various temperature variations, namely 55, 60, 65, 70 and 75 °C [29]. This study aims to determine the HAp/CTS composite with a high adsorption capacity so that it is used as an adsorbent in the adsorption of Cu^{2+} and Pb^{2+} ions. Testing of adsorption capacity by HAp/CTS composite can be seen in Table 3.

Table 3 shows that the highest adsorption capacity value is found in the HAp/CTS 65°C composite for both ions of 1.9979 mg/g for Cu^{2+} ions and 0.9965 mg/g for Pb^{2+} ions. The HAp/CTS 65°C composite will be used as an adsorbent in the adsorption of Cu^{2+} and Pb^{2+} ions. The

Table 3. Adsorption capacity of Cu^{2+} and Pb^{2+} ions by HAp/CTS composite

Sample	q_e of Cu^{2+} (mg/g)	q_e of Pb^{2+} (mg/g)
HAp	1.9936	0.9909
HAp/CTS 55 °C	1.9942	0.9915
HAp/CTS 60 °C	1.9971	0.9952
HAp/CTS 65 °C	1.9979	0.9965
HAp/CTS 70 °C	1.9934	0.9912
HAp/CTS 75 °C	1.9966	0.9952

adsorption ability of the composite is determined by the particle size of the adsorbent. The particle size of the HAp/CTS composite can affect the surface area available for interaction with adsorbed substances. The smaller the particle size of the HAp/CTS composite, the more surface area is available, thus increasing the adsorption ability of the composite. The active side in the form of functional groups on the adsorbent can affect the adsorption ability. The surface of the adsorbent has active sides in the form of $-\text{NH}_2$ and $-\text{OH}$ groups that are able to form bonds with molecules on the adsorbate. The HAp/CTS 65 °C composite was be further characterized by FTIR, XRD, SEM-EDS, and SAA and will be used as an adsorbent in heavy metal ions (Cu^{2+} and Pb^{2+}) adsorption in this study.

FTIR Analysis

FTIR analysis aims to analyze the functional groups in the form of absorption peaks and molecular interactions that play a role in the synthesis of HAp, CTS, and HAp/CTS composites. FTIR analysis was carried out at wave numbers 4000–500 cm^{-1} . FTIR spectra of the synthesized HAp, CTS, and HAp/CTS composite can be seen in Fig. 2. The FTIR signal of HAp at 3277 cm^{-1} is the absorption band of the $-\text{OH}$ group. At wavenumber 1023 cm^{-1} , there is a PO_4^{3-} functional group with asymmetric stretching vibrations, then P–O functional groups, 598 cm^{-1} , and 560 cm^{-1} with O–P–O bending vibrations [23]. The FTIR spectrum shows the characteristic bands of CTS. The C–H functional group at 2873 cm^{-1} with stretching vibrations, O–H functional group at 3433 cm^{-1} with stretching vibrations. At wavenumber 1620 cm^{-1} , there is a C=O group with stretching vibrations, and an N–H group is present at

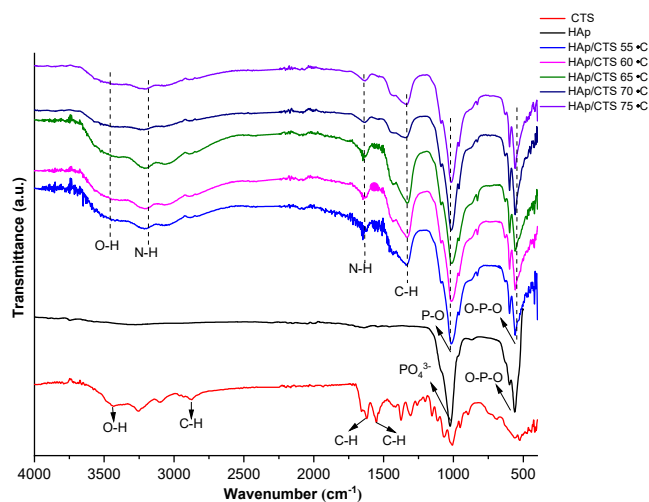


Fig 2. FTIR spectra of cuttlefish bone, HAp, CTS, and HAp/CTS composite

1552 cm^{-1} with bending vibrations. The FTIR spectrum of HAp/CTS composite with temperature variation states that there are all absorption bands for HAp and CTS. The O-H functional group of the HAp/CTS (55, 60, 65, 70, 75 $^{\circ}\text{C}$) composite at 3429, 3417, 3433, 3464 and 3489 cm^{-1} respectively. A shift of some characteristic peaks occurred. The shifting of -OH band absorption showed an interaction between HAp and CTS through hydrogen bonds, as displayed in Fig. 3 [30]. The P-O asymmetric stretching vibration moved from 1023 to 1018 cm^{-1} . Moreover, O-P-O bending vibrations shifted from 561 to 559 cm^{-1} . The decrease in intensity and widening of the peak is also assumed because of the interaction between the composite constituents, such as hydrogen bonding between HAp and CTS, as shown in Fig. 4 [30].

XRD Analysis

XRD analysis was performed to determine the crystallinity level of HAp and HAp/CTS composites by comparing the data obtained with the HAp standard (ICDS#157481) from the resulting diffraction pattern, the structure, orientation, and crystal size of the sample. In addition, this XRD analysis is also used to determine the size of the sample through Scherer calculation (Eq. (4));

$$L = \frac{k\lambda}{\beta \cos \theta} \quad (4)$$

where L = crystal size (nm); k = constant (0.9); λ = X-ray wavelength; β = full width at half maximum (FWHM) at

2θ (π 180); θ B = Bragg angle.

Based on the XRD graph, the diffraction pattern of standard HAp with (ICDS #157481) (Fig. 4(a)) corresponds to the diffraction pattern of the synthesized cuttlefish bone HAp (Fig. 4(b)). It can be seen at 2θ peaks with values of 24.5 $^{\circ}$; 30.7 $^{\circ}$; 32.3 $^{\circ}$; and 38.7 $^{\circ}$. Fig. 4(c) is the XRD spectrum of the HAp/CTS 65 $^{\circ}\text{C}$ composite. There is a new peak, which is the CTS peak. The CTS characteristic peak is located at 19.34 $^{\circ}$. CTS has a typical peak at 10 $^{\circ}$ -20 $^{\circ}$ [23]. In the HAp/CTS 65 $^{\circ}\text{C}$ composite, there was a peak shift due to several factors, namely crystal lattice stretching or shrinking, atomic substitution, particle size, chemical composition, and temperature. The XRD spectra for the HAp/CTS 65 $^{\circ}\text{C}$ composite showed that the crystallinity of HAp decreased with the addition of CTS polymer. The decrease in crystallinity and crystal size is proportional to the decrease in HAp content in the composite, which

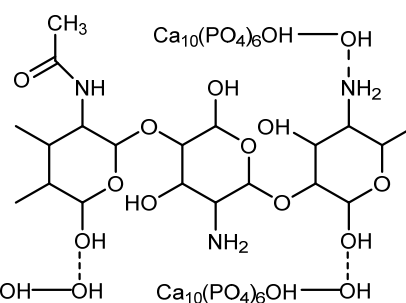


Fig 3. Proposed interaction between hydroxyapatite and chitosan [30]

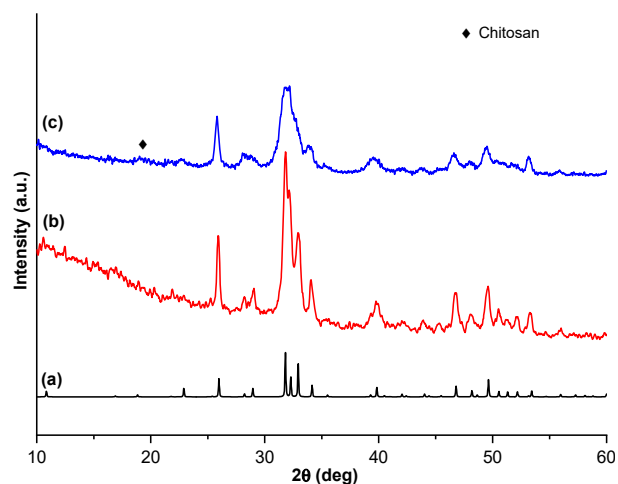


Fig 4. XRD spectra of (a) standard HAp, (b) cuttlefish bone HAp, and (c) HAp/CTS 65 $^{\circ}\text{C}$ composite

is indicated by the broadening of the diffraction peaks. The formation of a double diffraction pattern between HAp and CTS in the diffractogram states that the HAp/CTS 65 °C composite has been successfully synthesized. Based on Scherrer equation calculation, cuttlefish bone HAp and HAp/CTS 65 °C composite have crystal sizes of 23.60 and 13.82 nm, respectively.

SEM-EDS Analysis

SEM analysis was performed to characterize the surface morphology. SEM-EDS testing was conducted to analyze the surface morphology and elemental analysis of the HAp/CTS 65 °C composite. Fig. 5 is the morphology of the HAp/CTS 65 °C composite with magnifications of 5,000×, 10,000×, 20,000× and 50,000×. Fig. 5(a-d) shows the agglomerated chunk particles. This is due to the addition of CTS to HAp. The same results found that adding CTS to the composite formed chunks or granules with a rough surface. Then, the EDS results show the presence of HAp and CTS in the composite sample. This is characterized by Ca, C, O, P, and N elements with a Ca/P ratio of 1.61. The value is smaller than the Ca/P of HAp, which is 1.67. The EDS spectrum of the HAp/CTS 65°C composite can be seen in Fig. 5(e). Fig. 6 displays the

particle size distribution of the HAp/CTS 65 °C composite. The particle size distribution range of the HAp/CTS 65 °C composite produced ranges from 1–80 μm with an average size of 4.257 μm.

SSA Analysis

The surface area value of HAp/CTS 65 °C composite is 40.8858 m²/g. BET surface area is influenced by one factor that affects the adsorption ability

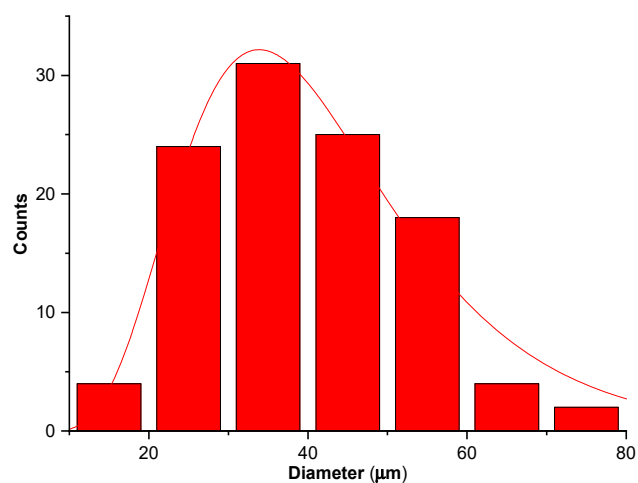


Fig 6. Particle size distribution of HAp/CTS 65 °C composite

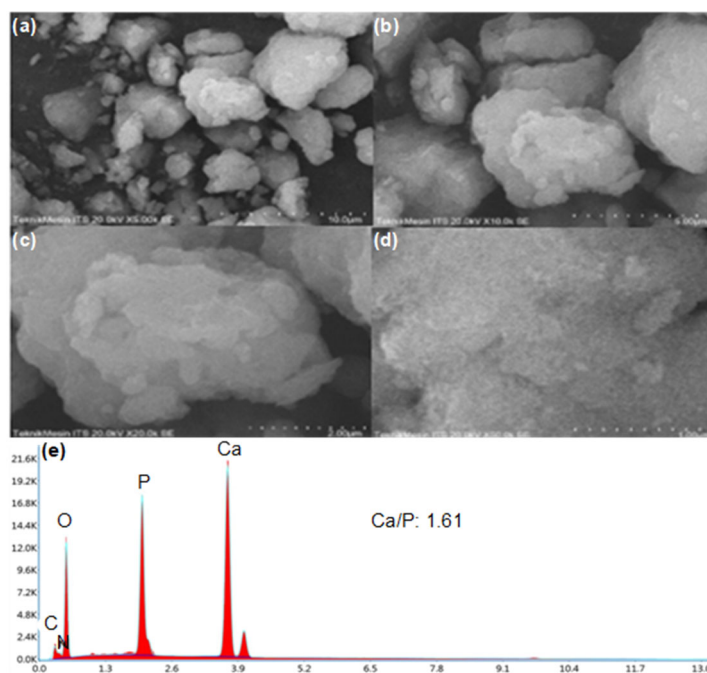


Fig 5. SEM photographs of HAp/CTS 65 °C composite: (a) 5,000×, (b) 10,000×, (c) 20,000×, and (d) 50,000× magnification and (e) EDS spectrum of HAp/CTS 65 °C composite

of a material. Other factors such as pore size, pore structure, surface chemical properties, and interaction between adsorbent compounds and adsorbed substances are also influential in determining the effectiveness of adsorption [23].

Adsorption Isotherm Analysis of Cu²⁺ and Pb²⁺ Ions

The adsorbent used for adsorption isotherm is HAp/CTS 65 °C composite with various concentration variations of Cu²⁺ and Pb²⁺ solutions, namely 200, 400, 600, 800, and 1000 mg/L. The following Langmuir and Freundlich isotherm graphs can be seen in Fig. 7 and 8. The linear equation can determine the adsorption capacity (q_m) from the slope value and the Langmuir

isotherm constant (K_L) from the intercept value. Then, from the linear equation, the adsorption intensity value (n) can be determined from the slope value and the Freundlich adsorption capacity value (K_F) from the intercept value. The adsorption isotherm analysis that has been carried out produces data such as in the table.

Adsorption isotherms are used to explain the interactions that occur between ions and composites. Fig. 7–8 and Table 4 show the adsorption results for both Cu²⁺ and Pb²⁺ ions using HAp/CTS 65 °C composite. It is known that Cu²⁺ ions for Langmuir isotherm obtained an R² value of 0.9344 and Freundlich isotherm of 0.8741. While, Pb²⁺ ions for Langmuir isotherm obtained an R² value of 0.9811 and Freundlich isotherm of 0.8403.

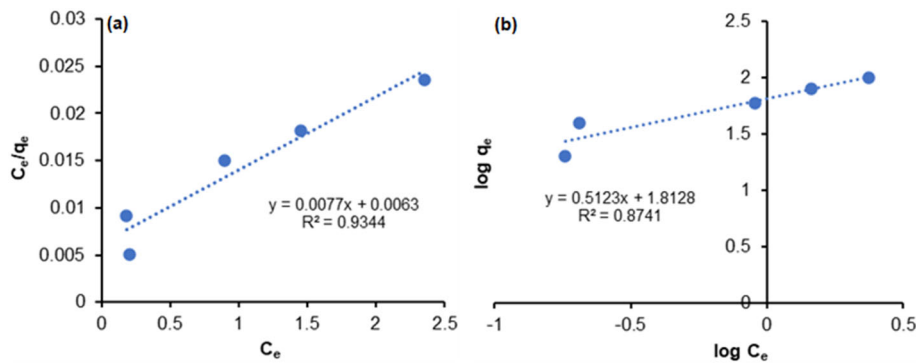


Fig 7. Linear graphs of (a) Langmuir and (b) Freundlich isotherms for Cu²⁺ ion sorption by HAp/CTS 65 °C composite

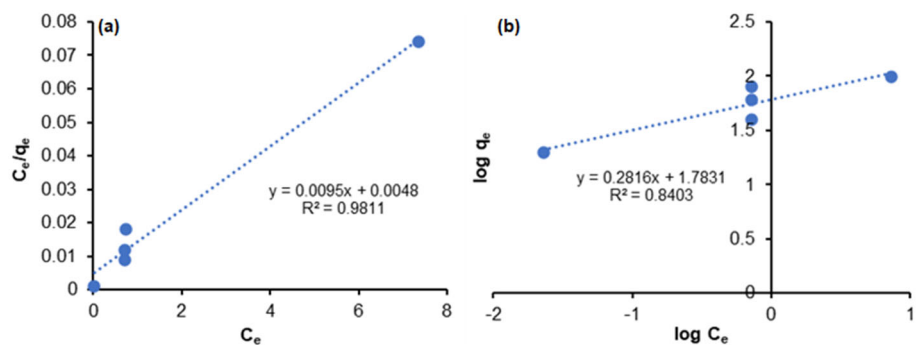


Fig 8. Linear graphs of (a) Langmuir and (b) Freundlich isotherms for Pb²⁺ ion sorption by HAp/CTS 65 °C composite

Table 4. Adsorption isotherm parameters of Cu²⁺ and Pb²⁺ ions on HAp/CTS 65 °C composite

Isotherm model	Parameter	Value of Cu ²⁺	Value of Pb ²⁺
Langmuir	q _m	129.8700	105.2600
	K _L	1.2220	1.9791
	R ²	0.9344	0.9811
Freundlich	K _F	64.9830	60.6870
	1/n	0.5123	0.2816
	R ²	0.8741	0.8403

The Langmuir isotherm equation is determined by the K_L value and the q_m value to determine the maximum adsorption capacity of the solid surface. In this study, the K_L value of adsorption of Cu^{2+} and Pb^{2+} ions by HAp/CTS 65 °C composite was 1.2220 and 1.9791, respectively. The positive K_L value indicates that the data obtained follows the Langmuir equation. This suggests that the composite is more likely to follow the Langmuir isotherm, where absorption occurs in one layer or monolayer and absorption of metal ions appears on a homogeneous surface. Then, the q_m value obtained was 129.87 mg/g for Cu^{2+} ions and 105.26 mg/g for Pb^{2+} ions. The q_m value indicates the maximum adsorption capacity of the solid surface. The q_m value will depend on the nature of the concrete surface and the type of molecules adsorbed. The greater the q_m value, the greater the number of molecules adsorbed on the surface of the solid. From these results, it can be assumed that Cu^{2+} and Pb^{2+} ions with HAp/CTS 65 °C composite tend to follow the Langmuir isotherm,

where the adsorption process occurs chemically on a homogeneous adsorbent surface in the form of a monolayer [23]. Chemical adsorption occurs due to molecules or atoms interacting chemically with the surface of the solid, forming chemical bonds with atoms or molecules on the surface. In chemical adsorption, the interactions can be powerful and specific. Adsorbed molecules can react chemically with atoms or molecules on the surface of the solid, forming covalent or other chemical bonds [31].

Analysis of Cu^{2+} and Pb^{2+} Ion Adsorption Kinetics

In determining the adsorption kinetics model of Cu^{2+} and Pb^{2+} ions by HAp/CTS 65 °C composite. This research also uses 2 types of kinetic models: pseudo-first-order and pseudo-second-order. The following kinetic curves of the HAp/CTS 65 °C composite can be seen in Fig. 9 and 10. Based on Fig. 9 and 10., it shows that the adsorption of Cu^{2+} and Pb^{2+} ions using HAp/CTS 65 °C

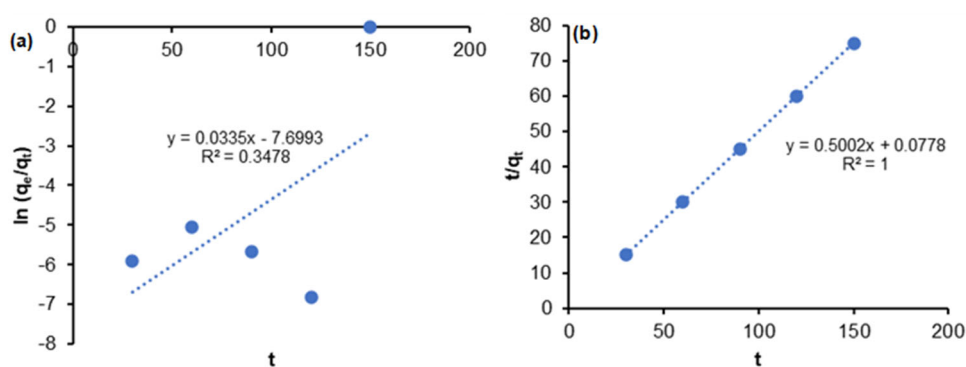


Fig 9. Linear graphs of (a) pseudo-first-order kinetics and (b) pseudo-second-order kinetics models on Cu^{2+} ion sorption by HAp/CTS 65 °C composite

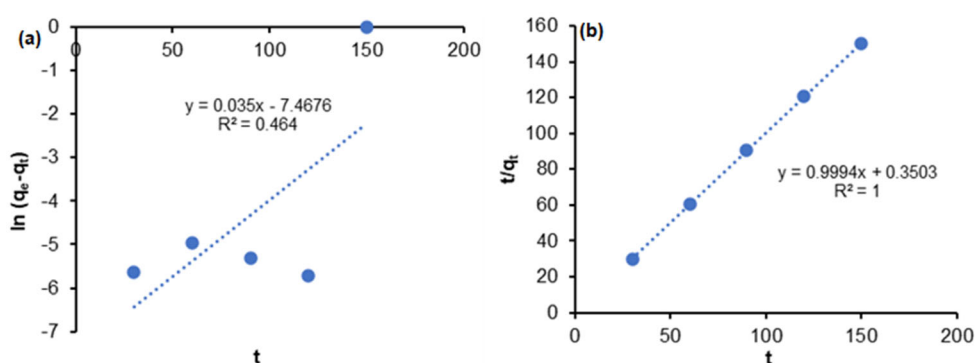


Fig 10. Linear graphs of (a) pseudo-first-order kinetics and (b) pseudo-second-order kinetics models on Pb^{2+} ion sorption by HAp/CTS 65 °C composite

Table 5. Kinetics model parameters of adsorption of (a) Cu^{2+} and (b) Pb^{2+} ions by HAp/CTS 65 °C composite

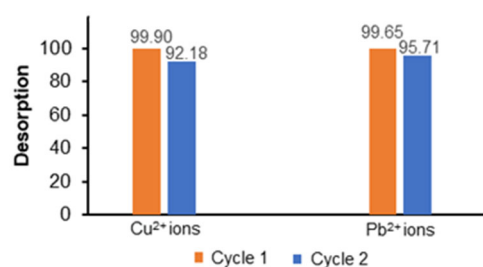
Adsorbent	Pseudo-first-order			Pseudo-second-order		
	q_e (mg/g)	k_1 (min^{-1})	R^2	q_e (mg/g)	k_2 (min^{-1})	R^2
HAp/CTS composite 65°C on Cu^{2+} ions	0.00046	-0.03350	0.34780	1.99920	3.21590	1.00000
HAp/CTS composite 65°C on Pb^{2+} ions	0.00054	-0.03500	0.46400	1.00060	2.85180	1.00000

composite follows the pseudo-second-order kinetics model. This is indicated by the R^2 value which is second-order larger than the pseudo-first-order kinetics, namely with R^2 values of 1 and 0.3478 for Cu^{2+} ions and R^2 values of 1 and 0.4640 for Pb^{2+} ions, respectively. The gas or liquid phase adsorption process follows the pseudo-second-order kinetics model, so chemical interactions occur in the adsorption process [32]. Therefore, it can be assumed that the governing interaction during the adsorption of Cu^{2+} and Pb^{2+} ions by HAp/CTS 65 °C composite is a chemical interaction. The analysis of adsorption kinetics produced data, as shown in Table 5.

Table 5 shows the adsorption of Cu^{2+} and Pb^{2+} ions with HAp/CTS 65 °C composite at pseudo-first-order, the q_e value of 0.00046 mg/g with k_1 value of -0.0335 min^{-1} for Cu^{2+} ions and q_e value of 0.00054 mg/g with k_1 value of -0.0350 min^{-1} for Pb^{2+} ions were obtained. The q_e value is the maximum adsorption capacity value and k_1 is the constant value of the adsorption rate. In the pseudo-second-order, q_e value of 1.9992 mg/g was obtained with k_2 value of 3.2159 g/mg.min. It can be concluded that the adsorption of Cu^{2+} and Pb^{2+} ions follow the pseudo-second-order model, and the interactions that occur in the adsorption of Cu^{2+} and Pb^{2+} ions with HAp/CTS 65 °C composite are chemical interactions [32].

Reusability Analysis of Cu^{2+} and Pb^{2+} Ions

The adsorption-desorption (reusability) study in this research was conducted to determine the reusability and efficiency of HAp/CTS 65 °C composite in adsorbing Cu^{2+} and Pb^{2+} ions. Reusability is very important in adsorbent applications because it reduces costs and increases process efficiency. The desorption agent for the HAp/CTS 65 °C composite was distilled water. The selected desorption agent should be effective, harmless to the biosorbent, not cause environmental pollution, and low cost [33]. Desorption agents serve to remove contaminants adsorbed on the adsorbent. The adsorption-desorption cycle of Cu^{2+}

**Fig 11.** Adsorption cycle of Cu^{2+} and Pb^{2+} ions by HAp-CTS 65 °C composite

and Pb^{2+} ions by HAp/CTS 65 °C composite is shown in Fig. 11.

Fig. 11 shows the results of the reusability analysis of HAp/CTS 65 °C composite in adsorbing Cu^{2+} and Pb^{2+} ions. HAp/CTS 65 °C composite has the potential to adsorb Cu^{2+} and Pb^{2+} ions until the second cycle of 99.89% and 92.18% for Cu^{2+} ions, 99.65% and 95.71% for Pb^{2+} ions. The decrease in the percentage of adsorption is due to the increase in cycles. The active sites on the adsorbent are saturated by Cu^{2+} and Pb^{2+} ion molecules. In addition, the adsorbent began to degrade at extreme pH conditions and blockage of pores and active sides on the adsorbent surface [34]. So, it can be concluded that the HAp/CTS 65 °C composite has a performance that still needs to be improved to be used repeatedly.

CONCLUSION

Synthesis of HAp/CTS composite, which consists of HAp derived from cuttlefish bone and CTS derived from shrimp shell, was successfully carried out using *in-situ* method. The HAp/CTS composite synthesized at 65 °C was selected for characterization and adsorption applications because it showed higher mass during the composite formation process and the highest adsorption capacity. SAA analysis of the HAp/CTS 65 °C composite showed a surface area of 40.8858 m^2/g . The use of HAp/CTS 65 °C composite in the adsorption of Cu^{2+} and Pb^{2+} ions follows the Langmuir isotherm model, which

shows the formation of a monolayer and follows the pseudo-second-order kinetic model. This research proves that the adsorption of Cu^{2+} and Pb^{2+} ions by HAp/CTS composite adsorbent has been successfully carried out. However, the reusability test results of the HAp/CTS 65 °C composite only succeeded up to 2 cycles.

■ ACKNOWLEDGMENTS

The author would like to thank LPPM (*Lembaga Penelitian dan Pengabdian Kepada Masyarakat*) of Universitas Andalas for supporting the researcher to publish this work.

■ CONFLICT OF INTEREST

The authors declare that they have no known competing financial interests or personal relationships that could have appeared to influence the work reported in this paper.

■ AUTHOR CONTRIBUTIONS

Novesar Jamarun conducted the experimental, Tri Yupi Amirullah drafted the manuscript, Novesar Jamarun, Syukri, Arika Prasejati, Wulandari, Sintia Caniago, Nabiila Ayyu Trycahyani wrote and revised the manuscript. All authors read and approved of the final manuscript.

■ REFERENCES

- [1] Basem, A., Jasim, D.J., Majdi, H.S., Mohammed, R.M., Ahmed, M., Al-Rubaye, A.H., and Kianfar, E., 2024, Adsorption of heavy metals from wastewater by chitosan: A review, *Results Eng.*, 23, 102404.
- [2] Jaffar, F.H., Othman, M.H.D., Ismail, N.J., Puteh, M.H., Kurniawan, T.A., Abu Bakar, S., and Abdullah, H., 2024, Hydroxyapatite-based materials for adsorption, and adsorptive membrane process for heavy metal removal from wastewater: Recent progress, bottleneck and opportunities, *J. Taiwan Inst. Chem. Eng.*, 164, 105668.
- [3] Singh, A., Sharma, A., Verma, R.K., Chopade, R.L., Pandit, P.P., Nagar, V., Aseri, V., Choudhary, S.K., Awasthi, G., Awasthi, K.K., and Sankhla, M.S., 2022, "Heavy Metal Contamination of Water and Their Toxic Effect on Living Organisms" in *The Toxicity of Environmental Pollutants*, Eds. Dorta, D.J., and de Oliveira, D.P., IntechOpen, Rijeka, Croatia.
- [4] Serezli, R., Akhan, S., and Delihasan-Sonay, F., 2011, Acute effects of copper and lead on some blood parameters on Coruh trout (*Salmo coruhensis*), *Afr. J. Biotechnol.*, 10 (16), 3204–3209.
- [5] Hariani, P.L., Rachmat, A., Said, M., and Salni, S., 2021, Modification of fishbone-based hydroxyapatite with MnFe_2O_4 for efficient adsorption of Cd(II) and Ni(II) from aqueous solution, *Indones. J. Chem.*, 21 (6), 1471–1483.
- [6] Zaini, M.A.A., Okayama, R., and Machida, M., 2009, Adsorption of aqueous metal ions on cattle-manure-compost based activated carbons, *J. Hazard. Mater.*, 170 (2-3), 1119–1124.
- [7] Paulino, A.T., Guilherme, M.R., Reis, A.V., Tambourgi, E.B., Nozaki, J., and Muniz, E.C., 2007, Capacity of adsorption of Pb^{2+} and Ni^{2+} from aqueous solutions by chitosan produced from silkworm chrysalides in different degrees of deacetylation, *J. Hazard. Mater.*, 147 (1-2), 139–147.
- [8] Xu, H.Y., Yang, L., Wang, P., Liu, Y., and Peng, M.S., 2008, Kinetic research on the sorption of aqueous lead by synthetic carbonate hydroxyapatite, *J. Environ. Manage.*, 86 (1), 319–328.
- [9] Peng, X., Li, Y., Liu, S., Jiang, T., Chen, W., Li, D., Yuan, J., and Xu, F., 2021, A study of adsorption behaviour of Cu(II) on hydroxyapatite-coated-limestone/chitosan composite, *J. Polym. Environ.*, 29 (6), 1727–1741.
- [10] Bailliez, S., Nzihou, A., Bèche, E., and Flamant, G., 2004, Removal of lead (Pb) by hydroxyapatite sorbent, *Process Saf. Environ. Prot.*, 82 (2), 175–180.
- [11] Laccourreya, O., and Maisonneuve, H., 2019, French scientific medical journals confronted by developments in medical writing and the transformation of the medical press, *Eur. Ann. Otorhinolaryngol. Head Neck Dis.*, 136 (6), 475–480.
- [12] Jamarun, N., Prasejati, A., Zulhadjri, Z., Caniago, S., Amirullah, T.Y., Wulandari, W., and Sisca, V., 2024, Effect of chitosan concentration on hydroxyapatite/chitosan composite synthesis using

- the *in-situ* method as a dye adsorbent, *Kuwait J. Sci.*, 51 (4), 100252.
- [13] Jamarun, N., Amelia, D., Rahmayeni, R., Septiani, U., and Sisca, V., 2023, The effect of temperature on the synthesis and characterization of hydroxyapatite-polyethylene glycol composites by *in-situ* process, *Hybrid Adv.*, 2, 100031.
- [14] Tattanon, T., Arpornmaeklong, P., Ummartyotin, S., and Pongprayoon, T., 2021, Hydrothermal synthesis of biphasic calcium phosphate from cuttlebone assisted by the biosurfactant L-rhamnose monohydrate for biomedical materials, *ChemEngineering*, 5 (4), 88.
- [15] Ryu, G.U., Kim, G.M., Khalid, H.R., and Lee, H.K., 2019, The effects of temperature on the hydrothermal synthesis of hydroxyapatite-zeolite using blast furnace slag, *Materials*, 12 (13), 2131.
- [16] Jamarun, N., Miftahurrahmi, M., and Septiani, U., 2016, Synthesis of hydroxyapatite from Halaban Limestone by Sol-Gel method, *Res. J. Pharm., Biol. Chem. Sci.*, 7 (5), 2956–2961.
- [17] Mulyani, R., Mulyadi, D., and Yusuf, N., 2020, Chitosan membrane from shrimp shells (*Panaeus modonon*) as an antibacterial food, *J. Phys.: Conf. Ser.*, 1477 (7), 072006.
- [18] Pakizeh, M., Moradi, A., and Ghassemi, T., 2021, Chemical extraction and modification of chitin and chitosan from shrimp shells, *Eur. Polym. J.*, 159, 110709.
- [19] Hisham, F., Maziat Akmal, M.H., Ahmad, F.B., and Ahmad, K., 2021, Facile extraction of chitin and chitosan from shrimp shell, *Mater. Today: Proc.*, 42, 2369–2373.
- [20] Ersal, F.M., Nurlely, N., and Sari, Y.W., 2019, Synthesis and characterization of hydroxyapatite-chitosan composite in situ by microwave irradiation method, *J. Phys.: Conf. Ser.*, 1248 (1), 012080.
- [21] Liu, X., Guo, Y., Zhang, C., Huang, X., Ma, K., and Zhang, Y., 2022, Preparation of graphene oxide/4A molecular sieve composite and evaluation of adsorption performance for Rhodamine B, *Sep. Purif. Technol.*, 286, 120400.
- [22] Khathi, M.T., Farhood, A.T., and Issmer, A.H., 2016, Determination of some heavy metals in extraction of plants by using AAS Technique, *J. Nat. Sci. Res.*, 6 (8), 130–137.
- [23] Trung, T.S., Minh, N.C., Cuong, H.N., Phuong, P.T.D., Dat, P.A., Nam, P.V., and Hoa, N.V., 2022, Valorization of fish and shrimp wastes to nano-hydroxyapatite/chitosan biocomposite for wastewater treatment, *J. Sci.: Adv. Mater. Devices*, 7 (4), 100485.
- [24] Muñoz-Sanchez, E.R., Arrieta-Gonzalez, C.D., Quinto-Hernandez, A., Garcia-Hernandez, E., and Porcayo-Calderon, J., 2023, Synthesis of hydroxyapatite from eggshell and its electrochemical characterization as a coating on titanium, *Int. J. Electrochem. Sci.*, 18 (9), 100204.
- [25] Wulandari, W., Wellia, D.V., and Jamarun, N., 2021, The effect of pH on the synthesis and characterization hydroxyapatite from bamboo shell (*Sollen spp.*) with emulsion method, *J. Appl. Chem.*, 10 (6), 872–879.
- [26] Omar, B.A., Elmasry, R., Eita, A., Soliman, M.M., El-Tahan, A.M., and Sitohy, M., 2022, Upgrading the preparation of high-quality chitosan from *Procambarus clarkii* wastes over the traditional isolation of shrimp chitosan, *Saudi J. Biol. Sci.*, 29 (2), 911–919.
- [27] Miron, A., Sarbu, A., Zaharia, A., Sandu, T., Iovu, H., Fierascu, R.C., Neagu, A.L., Chiriac, A.L., and Iordache, T.V., 2022, A top-down procedure for synthesizing calcium carbonate-enriched chitosan from shrimp shell wastes, *Gels*, 8 (11), 742.
- [28] Jamarun, N., Putri, Z.R., Septiani, U., Yusuf, Y., Sisca, V., and Zilfa, Z., 2023, The effect of pH on the synthesis and characterization of hydroxyapatite-polyethylene glycol composites by *in-situ* process, *Rasayan J. Chem.*, 16 (3), 1796–1804.
- [29] Amalina, F., Abd Razak, A.S., Krishnan, S., Zularisam, A.W., and Nasrullah, M., 2022, A review of eco-sustainable techniques for the removal of Rhodamine B dye utilizing biomass residue adsorbents, *Phys. Chem. Earth*, 128, 103267.

- [30] Ait Said, H., Mabroum, H., Lahcini, M., Oudadesse, H., Barroug, A., Ben Youcef, H., and Noukrati, H., 2023, Manufacturing methods, properties, and potential applications in bone tissue regeneration of hydroxyapatite-chitosan biocomposites: A review, *Int. J. Biol. Macromol.*, 243, 125150.
- [31] Putri, K.N.A., Keereerak, A., and Chinpa, W., 2020, Novel cellulose-based biosorbent from lemongrass leaf combined with cellulose acetate for adsorption of crystal violet, *Int. J. Biol. Macromol.*, 156, 762–772.
- [32] Peng, X., Chen, W., He, Z., Li, D., Liu, H., Jin, H., Zhou, G., and Xu, F., 2019, Removal of Cu(II) from wastewater using doped HAP-coated-limestone, *J. Mol. Liq.*, 293, 111502.
- [33] Beni, A.A., and Esmaili, A., 2020, Biosorption, an efficient method for removing heavy metals from industrial effluents: A review, *Environ. Technol. Innovation*, 17, 100503.
- [34] Hevira, L., Zilfa, Z., Rahmayeni, R., Ighalo, J.O., and Zein, R., 2020, Biosorption of indigo carmine from aqueous solution by *Terminalia catappa* shell, *J. Environ. Chem. Eng.*, 8 (5), 104290.